Journal of Data Acquisition and Processing
ISSN: 1004-9037
https://sjcjycl.cn/
DOI: 10.5281/zenodo.7778486

MACHINING MECHANISM AND STABILITY PREDICTION IN FLAT-END MILL PROCESS OF SKD11 HARD STEEL

Nhu-Tung Nguyen[1,*], Pham Van Dong[2], Tien-Dung Hoang[3], Vu Dinh Toan[3], Nguyen Duc Luan[3], Le Van Phong[4]

[1*]HaUI Institute of Technology, Hanoi University of Industry, Vietnam
[2]Department of Science and Technology, Hanoi University of Industry
[3]School of Mechanical and Automotive Engineering, Hanoi University of Industry
[4]Faculty of Mechanical Engineering and Mechatronics, PHENIKAA University
***Corresponding Author:** Nhu-Tung Nguyen
*HaUI Institute of Technology, Hanoi University of Industry, Vietnam,
Email: tungnn@haui.edu.vn

Abstract

This study was performed to investigated the mechanism and stability prediction of flat-end milling process of SKD11 hard steel. The static milling force (MF) model, dynamic milling force (DML) model, milling vibration (MV) model, stabilily loble diagram (SLD) model were developed and proposed in this study. The values of milling force coefficients (MLCs) and dynamic structure parameters (DSPs) were determined based on the combination of theoretical and experimental method. In static analysis, the relationship was very close to the linear regression with high determination coefficients ($R^2 > 97\%$) in all three x, y, z directions. In milling process the SKD11 hard steel using flat-end mill cutter, with each dynamic system, the natural frequencies in different directions were quite close to each other but different. The natural frequency of machine-tool system was almost half of natural frequency of machine-workpiece system. The width of the stability region increased when the spindle speed increased. The machining processes were almost at the stable conditions with the axial depth of cut to be smaller than 0.3 mm at all values of spindle speed. The stable and unstable conditions in milling processes were verified with high precision for almost milling tests. With the points at the border between stable and unstable zones, the verified results had small different point between the predicted results using the proposed model and the analyzed results from experimental processes.

Keywords: Milling mechanism, milling forces, Milling vibration; Dynamic Structure

1. Introduction

The cutting processes have been conducted by many different methods such as milling, turning, drilling, etc. in which, milling is one of the most used methods to machine the parts with high precision and good surface quality. The accuracy and surface quality of the machined surface depend on many parameters such as geometrical and material parameters of the cutting tool, cutting parameters, vibrations, friction, natural frequency, stiffness, and damping ratio of the technology system[1-3]. In particular, one of the parameters that greatly influence on the quality of the machining process is vibration.

Vibration is an integral part of any machining process. Machine builders, machine operators using the modern machines are always well aware of the adverse effects of vibration. Machine vibration can destabilize the machining process and can lead to chatter phenomenon that has a serious impact on the quality of the machining process, the life of the tool, and machine and tool machinability, etc. Vibration has a great influence on the productivity and quality of the machining processes[1-4]. Excessive vibration or chatter can lead to poor machined surface quality or damage the machine spindle bearings[1,4-6].

In the machining processes, the chatter and unstable phenomenon affect on the characteristics of the machining process such as reducing the quality of the machining process, increasing the cutting force, and increasing the vibration, increase cutting power, reduce the tool life, and have a negative effect on the structure of the technological system[7-10].

The studies that have been conducted to predict the occurrence of chatter phenomena to choose a reasonable machining parameters to overcome the above limitations will contribute to increase the productivity and quality of the machining process, especially in the milling process[10, 11].

Therefore, the studies that have been performed to determine the stable conditions for the machining process will be an important basis for the selection of the machining parameters to take the advantage of the capabilities of the technological system while still ensuring the requirements on the machined surface quality in the machining processes[12, 13].

Thus, the studies about the chatter prediction and the stable condition prediction are of great significance in the machining processes. The obtained results have been contributed to improving productivity and quality in the manufacturing process, especially in the mass production process. And, therefore, many scientists have focused to study and apply the investigated results on the chatter phenomenon and on the stable condition prediction in the machining process[12-15].

To simplify the mechanism of the milling processes, simplify the chatter phenomenon prediction and the stable, and unstable phenomenon prediction, the previous studies often have been assumed that the machine-workpiece system was absolutely rigid. That means the workpiece is absolutely fixed on the machine table. And so the vibrations of the machine-workpiece system are negligible[1-3, 16-18].

In fact, the machine-workpiece system is also a vibration system, so the machine-workpiece system affects on the characteristics of the dynamics systems of the machining processes. This study was conducted to determine the dynamics characteristics of the milling process including static milling forces (MFs), dynamic milling forces (DMFs) and milling vibrations (MVs) of the milling process, determining the milling force coefficients (MFCs), determining structural dynamic parameters (SDPs) of the machine-tool system and the machine-workpiece system, predicting the stable domain and checking the model predicting the stability lobe digram (SLD) in the milling process of the SKD11 hard steel.

2. Theoretical of Flat-end Milling Mechanism and Stability prediction

2.1. Theoretical of Static Flat-end Milling Process

In flat-end mill process, at one cutting point in the cutting edge, the instantaneous differential milling forces (MFs) are described in Fig. 1 and can be calculated by Eq. (1)[19].

$$\begin{cases} dF_{t,j}(\phi, z) = K_{te} * dz + K_{tc} * h_j(\phi_j(z)) * dz \\ dF_{r,j}(\phi, z) = K_{re} * dz + K_{rc} * h_j(\phi_j(z)) * dz \\ dF_{a,j}(\phi, z) = K_{ae} * dz + K_{ac} * h_j(\phi_j(z)) * dz \end{cases} \quad (1)$$

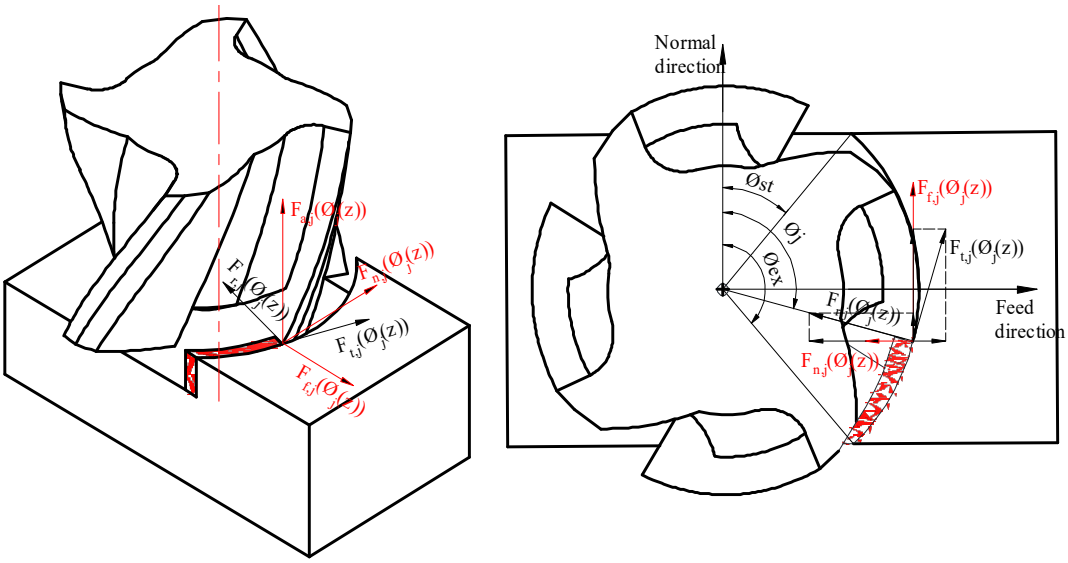

Fig. 1. Instantaneous differential MFs

where K_{ij} are the milling force coefficients (MFCs), dz is the differential axial depth of cut, $h_j(\phi_j(z))$ that is the undeform instantaneous static chip thickness at the cutter rotation angle ($\phi_j(z)$) can be calculated by Eq. (2).

$$h_j\left(\phi_j(z)\right) = f_t sin\phi_j(z) \quad (2)$$

where f_t is the feed per flute.

So, the differential MFs can be written by Eq. (3).

$$\begin{cases} dF_{t,j}(\phi, z) = \left[K_{tc} f_t \sin\phi_j(z) + K_{te}\right] * dz \\ dF_{r,j}(\phi, z) = \left[K_{rc} f_t \sin\phi_j(z) + K_{re}\right] * dz \\ dF_{a,j}(\phi, z) = \left[K_{ac} f_t \sin\phi_j(z) + K_{ae}\right] * dz \end{cases} \quad (3)$$

The MFCs can be determined by Eq. (4).

$$\begin{cases} K_{tc} = \dfrac{C_1\bar{F}_{fc} - C_2\bar{F}_{nc}}{C_1^2 + C_2^2} & K_{te} = \dfrac{C_3\bar{F}_{fe} - C_4\bar{F}_{ne}}{C_3^2 + C_4^2} \\ K_{rc} = \dfrac{C_2\bar{F}_{fc} + C_1\bar{F}_{nc}}{C_1^2 + C_2^2} & K_{re} = \dfrac{C_4\bar{F}_{fe} + C_3\bar{F}_{ne}}{C_3^2 + C_4^2} \\ K_{ac} = -\dfrac{\bar{F}_{ac}}{C_4} & K_{ae} = \dfrac{\bar{F}_{ae}}{C_5} \end{cases} \quad (4)$$

where the constants (C_1, C_2, C_3, C_4, and C_5) are determined based on the cutter geometry and the cutting condition parameters[19].
The linear components ($\bar{F}_{fc}, \bar{F}_{fe}, \bar{F}_{nc}, \bar{F}_{ne}, \bar{F}_{ac}$, and $\bar{F}_{ae}$) are determined depending on the linear relationship of average MFs and feed per flute and these values can be determined based on the milling experimental data of MFs.

2.2. Theoretical of Dynamic Flat-end Milling Process

In flat-end mill process, the undeform instantaneous chip thickness are calculated by Eq. (5)[20].

$$h_j\left(\phi_j(z)\right) = h_s\left(\phi_j(z)\right) + h_{run-o}\quad\left(\phi_j(z)\right) + h_d\left(\phi_j(z)\right) \quad (5)$$

where the static chip thickness is calculated by Eq. (6).

$$h_s\left(\phi_j(z)\right) = f_t \sin\left(\phi_j(z)\right) \quad (6)$$

The dynamic chip thickness is calculated by Eq. (7).

$$h_d\left(\phi_j(z)\right) = \left(w_t^c(\phi_j) - w_t^w(\phi_j)\right) - \left(w_{(t-\tau)}^c(\phi_j) - w_{(t-\tau)}^w(\phi_j)\right) \quad (7)$$

where $w_t^c(\phi_j)$ and $w_{(t-\tau)}^c(\phi_j)$ the displacements of machine-tool system at the cutter rotation angle $\phi_j(z)$ of the current and the previous tool passes, and they can be calculated by Eq. (8).

$$\begin{cases} w_t^c(\phi_j) = -x_t^c \sin\left(\phi_j(z)\right) - y_t^c \cos\left(\phi_j(z)\right) \\ w_{(t-\tau)}^c(\phi_j) = -x_{(t-\tau)}^c \sin\left(\phi_j(z)\right) - y_{(t-\tau)}^c \cos\left(\phi_j(z)\right) \end{cases} \quad (8)$$

where x_t^c and y_t^c are the machine-tool vibrations at the time (t) in x and y directions. And $x_{(t-\tau)}^c$ and $y_{(t-\tau)}^c$ are the machine-tool vibrations at the time $(t-\tau)$ in x and y directions.

$w_t^w(\phi_j)$ and $w_{(t-\tau)}^w(\phi_j)$ the displacements of machine-workpiece system at the cutter rotation angle $\phi_j(z)$ of the current and the previous tool passes, and they can be calculated by Eq. (9).

$$\begin{cases} w_t^w(\phi_j) = -x_t^w \sin\left(\phi_j(z)\right) - y_t^w \cos\left(\phi_j(z)\right) \\ w_{(t-\tau)}^w(\phi_j) = -x_{(t-\tau)}^w \sin\left(\phi_j(z)\right) - y_{(t-\tau)}^w \cos\left(\phi_j(z)\right) \end{cases} \quad (9)$$

where x_t^w and y_t^w are the machine-workpiece vibrations at the time (t) in x and y directions. And $x_{(t-\tau)}^c$ and $y_{(t-\tau)}^c$ are the machine-tool vibrations at the time $(t-\tau)$ in x and y directions. Then, the dynamic chip thickness can be calculated by Eq. (10).

$$h_d\left(\phi_j(z)\right) = \Delta x \sin\left(\phi_j(z)\right) + \Delta y \cos\left(\phi_j(z)\right) \qquad (10)$$

where

$$\begin{cases} \Delta x = \left(x_{(t-\tau)}^c - x_t^c\right) - \left(x_{(t-\tau)}^w - x_t^w\right) \\ \Delta y = \left(y_{(t-\tau)}^c - y_t^c\right) - \left(y_{(t-\tau)}^w - y_t^w\right) \end{cases} \qquad (11)$$

Assume that the used tool is a new tool, so the chip thickness component that is formed from the runout is negligible.

$$h_{run-out}\left(\phi_j(z)\right) = 0 \qquad (12)$$

So, the undeform instantaneous chip thickness are calculated by Eq. (13).

$$h_j\left(\phi_j(z)\right) = f_t \sin\left(\phi_j(z)\right) + \Delta x \sin\left(\phi_j(z)\right) + \Delta y \cos\left(\phi_j(z)\right) \qquad (13)$$

From above parameters, the instantaneous differential MFs can be predicted by a flow chart as described in Fig. 2[2, 3].

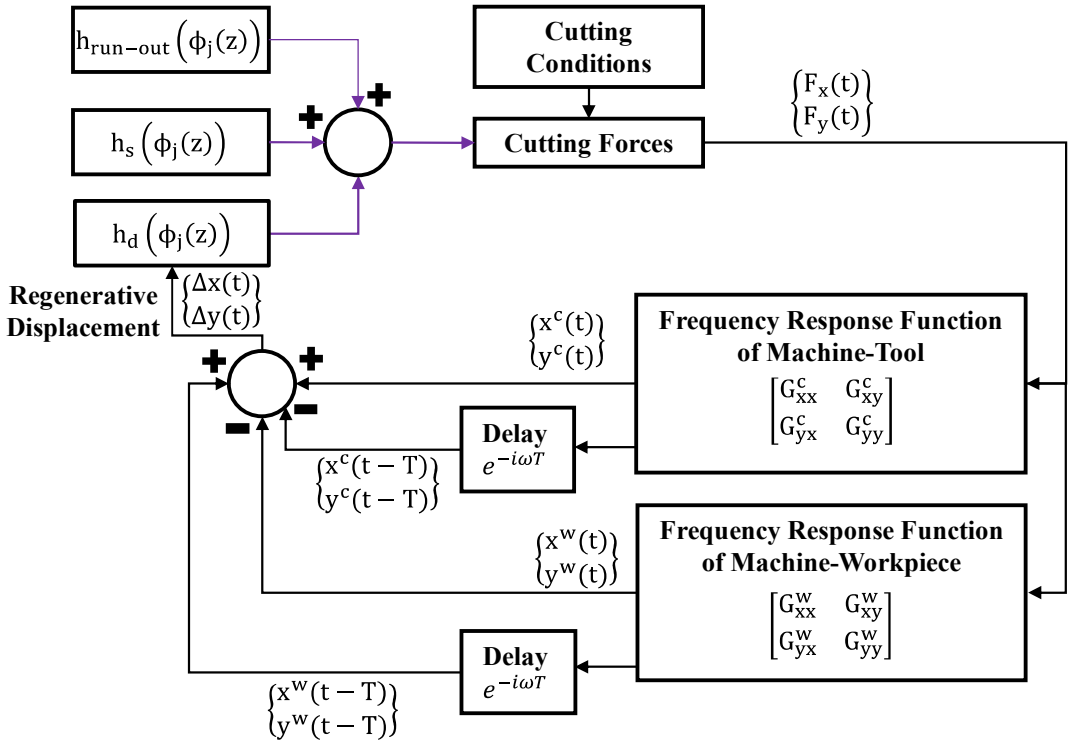

Fig.2. Flow chart to predict the MFs

2.2. Theoretical of Stability prediction

In milling processes, the stable cutting conditions are presented by Eq. (14)[1-3].

$$a_{lim} = \frac{2\pi}{N_t K_t}\Lambda_R(1+\mathcal{K}^2) \quad (14)$$

Where $N_t$is the number of cutting flutes on the cutter. K_t is the tangential cutting force coefficient. This value can be determined by combination method of theoretical and experimental milling processes.

Λ_R is the real part of the eigenvalue of the machine-tool-workpiece dynamic system. This part can be determined by Eq. (15).

$$\Lambda_{1,2} = \frac{-a_1 \pm \sqrt{a_1^2-4a_0}}{2a_0} = -\frac{1}{2a_0}\left(a_1 \pm \sqrt{a_1^2-4a_0}\right) \quad (15)$$

where

$$a_0 = \alpha_{xx}\alpha_{yy}G_{xx}G_{yy} - \alpha_{xy}\alpha_{yx}G_{xx}G_{yy} = G_{xx}G_{yy}\left(\alpha_{xx}\alpha_{yy} - \alpha_{xy}\alpha_{yx}\right) \quad (16)$$

and

$$a_1 = \alpha_{xx}G_{xx} + \alpha_{yy}G_{yy} \quad (17)$$

α_{ij} are the coefficients that can be determined by Eq. (18).

$$\begin{cases} \alpha_{xx} = \frac{1}{2}[\cos 2\phi + 2K_r\phi + K_r \sin 2\phi]_{\phi_{st}}^{\phi_{ex}} \\ \alpha_{xy} = \frac{1}{2}[-\sin 2\phi - 2\phi + K_r \cos 2\phi]_{\phi_{st}}^{\phi_{ex}} \\ \alpha_{yx} = \frac{1}{2}[-\sin 2\phi + 2\phi + K_r \cos 2\phi]_{\phi_{st}}^{\phi_{ex}} \\ \alpha_{yy} = \frac{1}{2}[-\cos 2\phi - 2K_r\phi - K_r \sin 2\phi]_{\phi_{st}}^{\phi_{ex}} \end{cases} \quad (18)$$

and G_{xx}, G_{yy} are the sum response frequency function (FRF) of machine-tool system and machine-workpiece system.

The ratio of the imaginary and the real part of eigenvalue ($\mathcal{K}$) can be determined by Eq. (19).

$$\mathcal{K} = \frac{\Lambda_I}{\Lambda_R} = \frac{\sin\omega_c T}{1-\cos\omega_c T} \quad (19)$$

The spindle speed can be determined depending on the chatter frequency (ω_c) by Eq. (20).

$$n = \frac{60}{N_t T} = \frac{60}{N_t\left\{\frac{1}{\omega_c}(\varepsilon + j.2\pi)\right\}} \quad (20)$$

where T is the flue pass period. ε is the different phase between the inner and outer modulations. This value can be determined by Eq. (21).

$$\varepsilon = \pi - 2\psi \quad (21)$$

where ψ is the phase of the eigenvalue that can be determined by Eq. (22).

$$\psi = \tan^{-1}(\mathcal{K}) \quad (22)$$

j is an integer corresponding to the vibration wave number within a flute period.

Then, the chatter vibrations can be determined depending on many parameters as described in Fig. 3[2, 3].

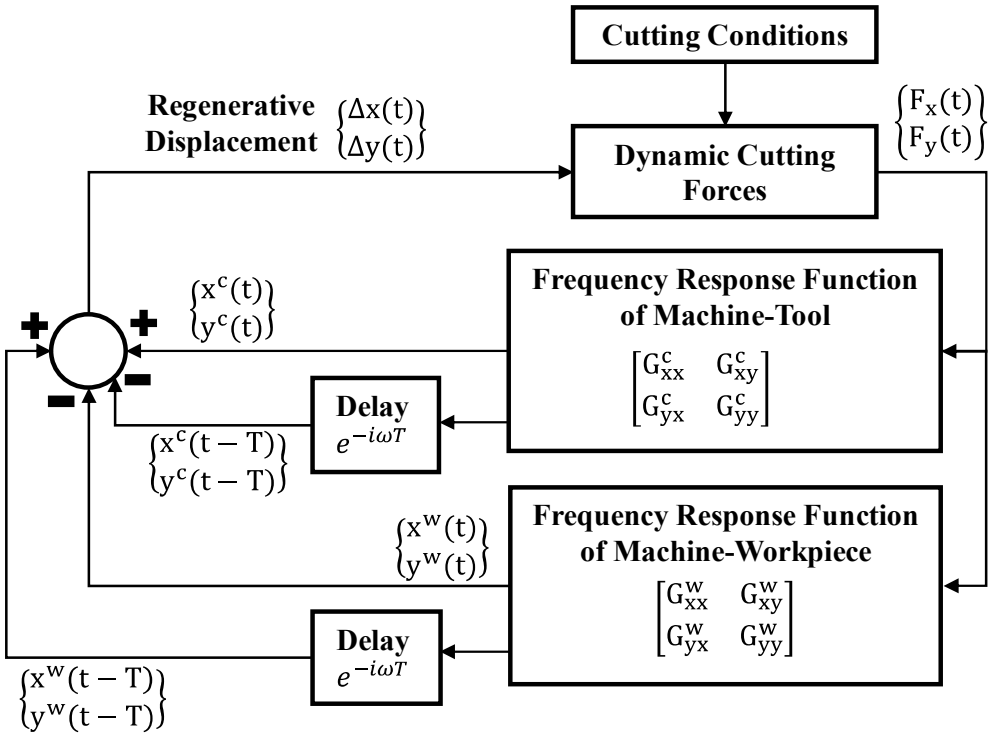

Fig.3. Flow chart to predict the chatter vibrations

In this figure, the regenerative displacements of machine-tool system and machine-workpiece system infrequency domain can be expresses by Eq. (23) and Eq. (24).

$$\begin{Bmatrix} \Delta x^c(i\omega) \\ \Delta y^c(i\omega) \end{Bmatrix} = (1 - e^{-i\omega T}) \begin{bmatrix} G^c_{xx} & G^c_{xy} \\ G^c_{yx} & G^c_{yy} \end{bmatrix} \begin{Bmatrix} F_x(i\omega) \\ F_y(i\omega) \end{Bmatrix} \quad (23)$$

and

$$\begin{Bmatrix} \Delta x^w(i\omega) \\ \Delta y^w(i\omega) \end{Bmatrix} = (1 - e^{-i\omega T}) \begin{bmatrix} G^w_{xx} & G^w_{xy} \\ G^w_{yx} & G^w_{yy} \end{bmatrix} \begin{Bmatrix} F_x(i\omega) \\ F_y(i\omega) \end{Bmatrix} \quad (24)$$

The cross components of the frequency response function are negligible ($G^{c,w}_{xy} = G^{c,w}_{yx} = 0$), the above equations can be simplified by Eq. (25) and Eq. (26).

$$\begin{cases} \Delta x^c(s) = (1 - e^{-sT}) G^c_{xx}(s) F_x(s) \\ \Delta y^c(s) = (1 - e^{-sT}) G^c_{yy}(s) F_y(s) \end{cases} \quad (25)$$

and

$$\begin{cases} \Delta x^w(s) = (1 - e^{-sT}) G^w_{xx}(s) F_x(s) \\ \Delta y^w(s) = (1 - e^{-s}) G^w_{yy}(s) F_y(s) \end{cases} \quad (26)$$

so,

$$\begin{Bmatrix} \Delta x(s) \\ \Delta y(s) \end{Bmatrix} = \begin{Bmatrix} \Delta x^c(s) - \Delta x^w(s) \\ \Delta y^c(s) - \Delta y^w(s) \end{Bmatrix} \quad (27)$$

and

$$\begin{Bmatrix}\Delta x(s)\\ \Delta y(s)\end{Bmatrix} = (1-e^{-sT})\begin{bmatrix}G_{xx}^{c}(s)-G_{xx}^{w}(s) & 0\\ 0 & G_{yy}^{c}(s)-G_{yy}^{w}(s)\end{bmatrix}\begin{Bmatrix}F_x(s)\\ F_y(s)\end{Bmatrix} \quad (28)$$

where $G_{xx}^{c}(s)$ and $G_{yy}^{c}(s)$ that are the FRFs of machine-tool system can be determined by Eq. (29).

$$\begin{cases} G_{xx}^{c}(s) = \dfrac{x^{c}(s)}{F_x(s)} = \dfrac{\omega_{ncx}^2}{k_{cx}(s^2+2\zeta_{cx}\omega_{ncx}s+\omega_{ncx}^2)} \\ G_{yy}^{c}(s) = \dfrac{y^{c}(s)}{F_y(s)} = \dfrac{\omega_{ncy}^2}{k_{cy}(s^2+2\zeta_{cy}\omega_{ncy}s+\omega_{ncy}^2)} \end{cases} \quad (29)$$

where ω_{nc} and ζ_c are the natural frequency and damping ratio of the machine-tool system, respectively. These values are calculated depending on the damping constant (c_i) and the mass (m_i) of the machine-tool system as presented by Eq. (30) and Eq. (31).

$$\begin{cases} \omega_{ncx} = \sqrt{\dfrac{k_{cx}}{m_{cx}}} \\ \zeta_{cx} = \dfrac{c_{cx}}{2\sqrt{k_{cx}m_{cx}}} \end{cases} \quad (30)$$

$$\begin{cases} \omega_{ncy} = \sqrt{\dfrac{k_{cy}}{m_{cy}}} \\ \zeta_{cy} = \dfrac{c_{cy}}{2\sqrt{k_{cy}m_{cy}}} \end{cases} \quad (31)$$

Similarly, the machine-workpiece system, the FRF and the dynamic structure parameters can be determined by Eq. (32) to Eq. (34).

$$\begin{cases} G_{xx}^{w}(s) = \dfrac{x^{w}(s)}{F_x(s)} = \dfrac{\omega_{nwx}^2}{k_{wx}(s^2+2\zeta_{wx}\omega_{nwx}s+\omega_{nwx}^2)} \\ G_{yy}^{w}(s) = \dfrac{y^{w}(s)}{F_y(s)} = \dfrac{\omega_{ncy}^2}{k_{wy}(s^2+2\zeta_{wy}\omega_{nwy}s+\omega_{nwy}^2)} \end{cases} \quad (32)$$

and

$$\begin{cases} \omega_{nwx} = \sqrt{\dfrac{k_{wx}}{m_{wx}}} \\ \zeta_{wx} = \dfrac{c_{wx}}{2\sqrt{k_{wx}m_{wx}}} \end{cases} \quad (33)$$

$$\begin{cases} \omega_{nwy} = \sqrt{\dfrac{k_{wy}}{m_{wy}}} \\ \zeta_{wy} = \dfrac{c_{wy}}{2\sqrt{k_{wy}m_{wy}}} \end{cases} \quad (34)$$

The dymamic milling process with four degrees of freedom can be described in Fig. 4[20] and can be modeled by Eq. (35).

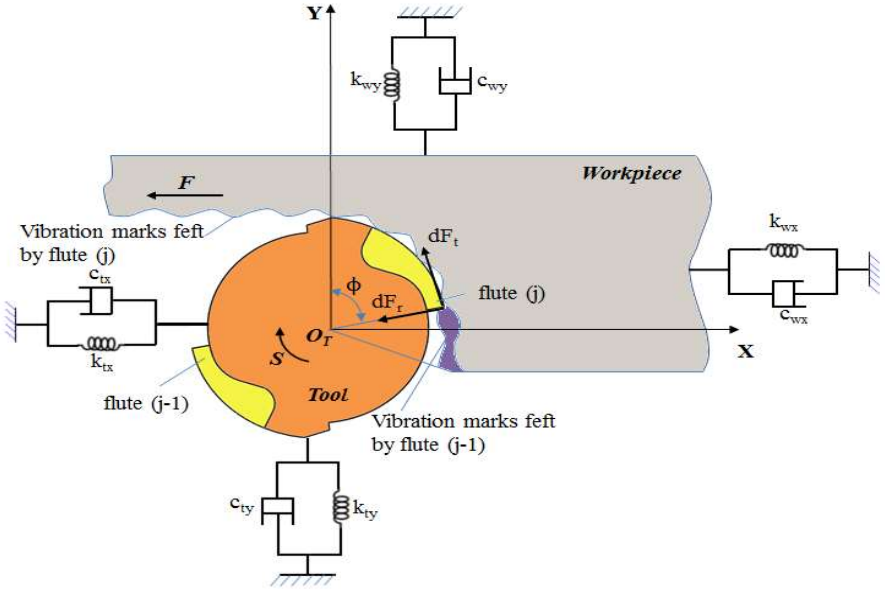

Fig.4. Dynamic milling process model

$$\begin{cases} m_{xt}\ddot{x}_t(t) + c_{xt}\dot{x}_t(t) + k_{xt}x_t = F_x(t) \\ m_{yt}\ddot{y}_t(t) + c_{yt}\dot{y}_t(t) + k_{yt}y_t = F_y(t) \\ m_{zt}\ddot{z}_t(t) + c_{zt}\dot{z}_t(t) + k_{zt}z_t = F_z(t) \\ m_{xw}\ddot{x}_w(t) + c_{xw}\dot{x}_w(t) + k_{xw}x_w = -F_x(t) \\ m_{yw}\ddot{y}_w(t) + c_{yw}\dot{y}_w(t) + k_{yw}y_w = -F_y(t) \\ m_{zw}\ddot{z}_w(t) + c_{zw}\dot{z}_w(t) + k_{zw}z_w = -F_z(t) \end{cases} \quad (35)$$

where x_t, y_t, and z_t are the machine-tool vibrations in x, y, and z directions, respectively. And x_w, y_w, z_w are the machine-workpiece vibrations in x, y, and z directions, respectively.

3. Material and Experimental Methods

A CNC milling machine (CNC HS Super MC500) was used to conduct the experiments. Several parameters of this CNC machine are maximum spindle speed of 30000 rpm, the power of spindle speed of 15 kW, the maximum feedrate in cutting of 30000 mm/min. The setup of experimental system includs machine, tool, workpiece, and measurement systems as described in Fig. 6 and Fig. 7.

The flat-end mill cutter HSSCo8 coated NiT (60HRC) was used in the experimental processes. These cutter has two flutes (teeth) with the diameter of 6 mm as decribed in Fig. 5.

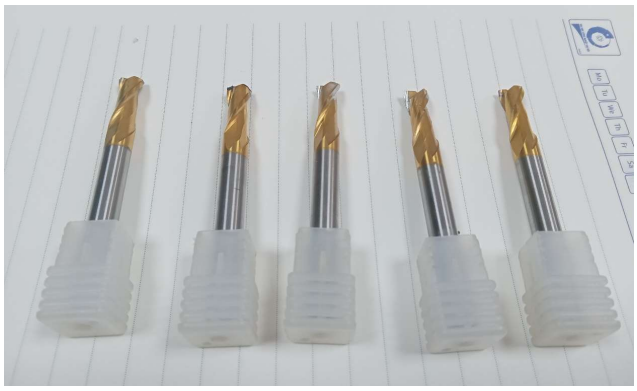

Fig.5. Milling tools

The hard steel workpiece (SKD11) after heat treatment to reach the hardess of 58 HRC was used in the experimental processes. The compositions of this steel are 1.5% of C, 0.25% of Si, 0.45% of Mn, 0.025% of P, 0.1% of S, 12.0% of Cr, 1.0% of Mo, 0.35% of V, and the remain component is the F. The dimensions of these workpieces were 80 x 40 x 40 mm as described in Fig. 6 and Fig. 7.

3.3. Measurement Systems

The dynamic structure parameter measurement system includes a signal processing equiment (LAN-XI) with four input and two ouput channels (51.2 kHz) of Bruel&Kjaer, Denmark. This measurement system uses the PULSE FFT 770 analysis modular of Bruel&Kjaer, uses an one-direction acceleration sensor (DeltaTron# Accelerometer 4513-B-002) and a tap hammer Types 8206 as described in Fig. 6.

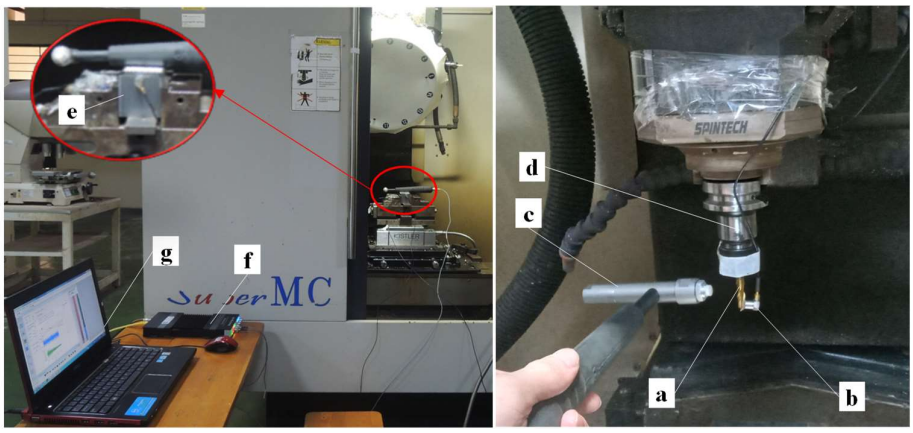

Fig.6. Experimental machine and measurement of dynamic structure parameters

The cutting force measurement system includes a three-direction dynamometer (Kistler Type 9139AA of Kisler, Switzerland), a signal processing system type 3160-B-042, and the DynoWare software. The vibrations in three directions were measured using a three-direction acceleration (Triaxial DeltaTron Accelerometer with TEDS Type 4525-B-001) with LAN-XI and the the PULSE FFT 770 analysis modular. The sutup of the cutting force and vibration measurement systems are described in Fig. 7.

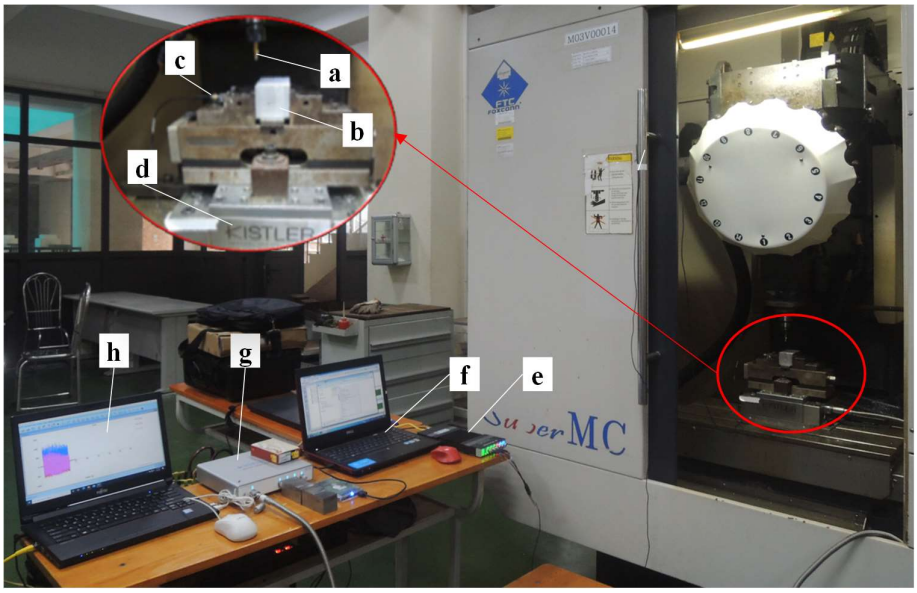

Fig.7. Measurement of MFs and MVs

4. Results and Discussion

4.1. Determination of Milling Force Coefficients and Verification of Milling Force Modeling

In this section, the milling experiments were performed to determine the MFCs. The average MFs were determine from the cutting tests with small vibrations. So, in these cases, the cutting tests were performed with milling conditions as following: The spindle speed was fixed as the constant value of 2000 rpm, the axial and radial depth of cut were also fixed at the values of 0.3 mm and 6 mm, respectively. Only the feed per flute were selected with the change from 0.050 mm/flute to 0.113 mm/flute (0.050, 0.063, 0.075, 0.088, and 0.113 mm/flute) to build the relationship between the average MFs and the feed per flute.

Depending on the MF data, the elationship between the average MFs and the feed per flute was build as illustrated in Fig. 8. It is clear that this relationship was very close to the linear regression with high determination coefficients ($R^2 > 97\%$) in all three x, y, z directions.

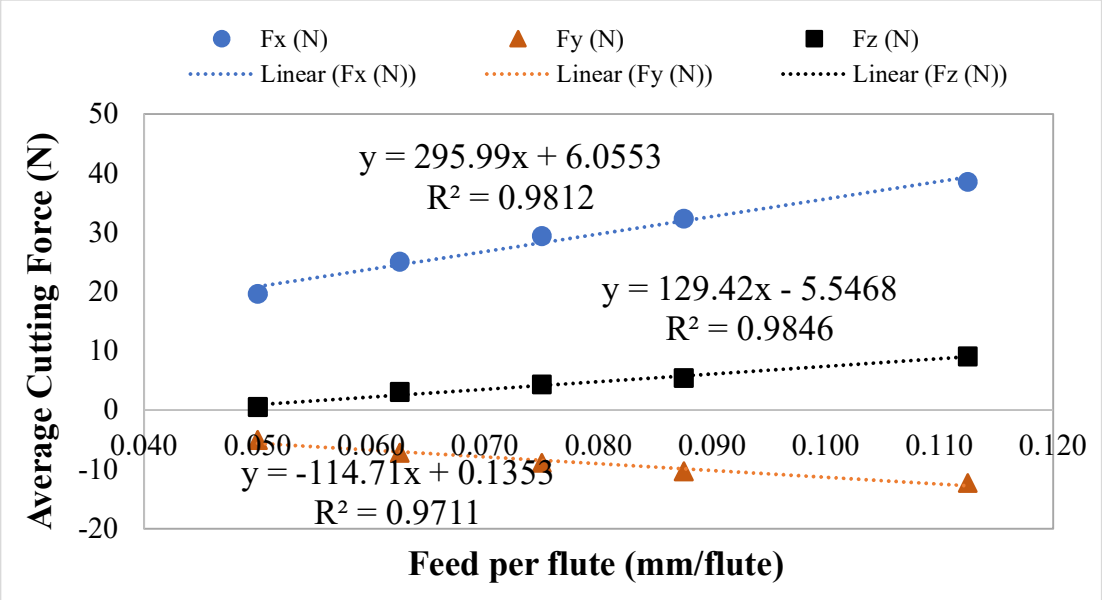

Fig.8. Average MFs and feed per flute relationship

So, in all three x, y, z directions, the relationships between the average MFs and the feed per flute were the linear functions. The constant values of these linear functions were applied to determine the values of MFC as listed in Table 1.

Table.1. The values of MFCs

Shear Force Coefficients (N/mm²)					**Edge Force Coefficients (N/mm)**		
K_{tc}	K_{rc}	K_{ac}	K_t	K_r	K_{te}	K_{re}	K_{ae}
2367.92	917.68	-815.795	2367.92	0.3876	24.831	1.1825	-14.482

From the determined values in table 9, it seems that the absolute values of shear MFCs are many times larger than the edge MFCs. So, the most important MFCs are the shear ones. And, in the shear MFCs, the tangential CFC (K_{tc} or K_t) was the most important one. This value was also used to predict the MFs and the SBL diagram as presented next sections.

4.2. Determination of Dynamics Structure Parameters and verification of Milling Force Models

The dynamic structure parameters of machine-tool system and machine-workpiece system were determined based on the analyzed results of the tapper tests with above measurement system. The stucture parameters of these dynamic systems include the system natural frequencies, system damping ratio, system stiffness, and system mass as listed in Table 2.

Table.2. The structure parameters of dynamic systems

Direction	**Frequency (Hz)**	**Damping ratio (%)**	**Model stiffness (N/m)**	**Mass (kg)**
Machine-ool System				
x	1119.8	1.835	1.64E+07	0.3314
y	1134.9	3.705	1.78E+07	0.2316

Machine-Workpiece System				
x	2790.6	3.940	1.43E+07	0.0466
y	2960.8	1.996	4.414E+07	0.1275

From the data in Table 2, it seems that with each dynamic system, the natural frequencies in different directions were quite close to each other but different. Besides, in these cases, the natural frequency of machine-tool system was almost half of natural frequency of machine-workpiece system. Using the obtained parameters, the compared results of the predicted dynamic MFs and the measured dynamic MFs in milling process of the SKD11 hard steel using a solid flat-end mill cutter are shown in Fig. 9.

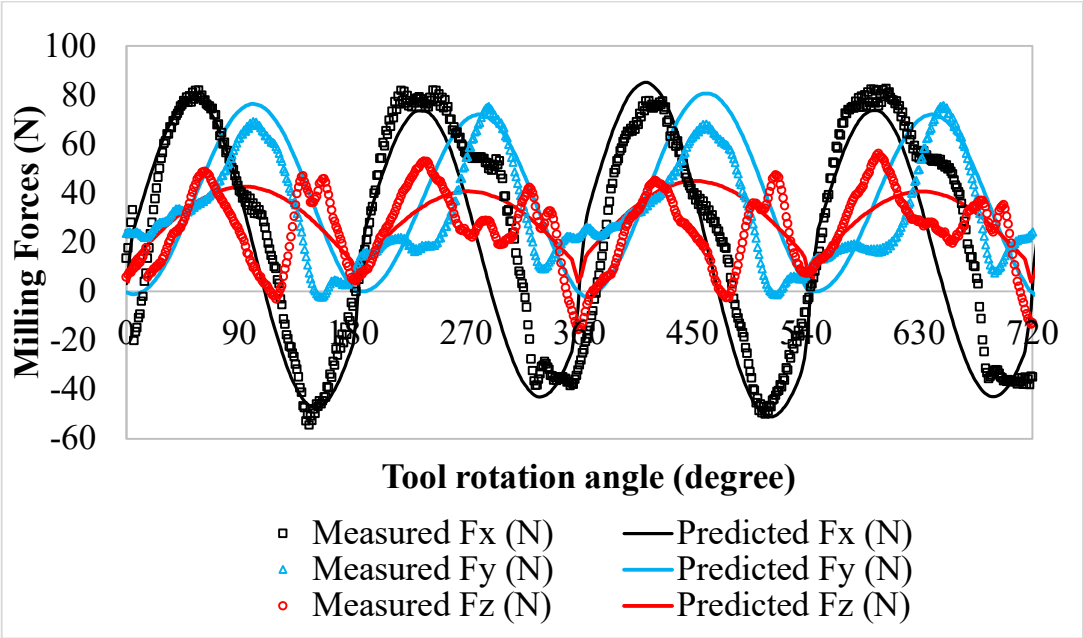

Fig.9. Predicted and experimental MFs

According to the angular position of the cutter, in all three directions including x, y, and z directions, the shape of the predicted dynamic MFs were very similar to the one of the measured dynamic MFs. In terms of values of MFs, on all three different directions, the values of the predicted dynamic MFs were also quite close to the values of the experimental dynamic MFs. However, there are still some differences between the predicted dynamic MFs and the experimentally measured MFs as depicted in Fig. 9.

4.3. Stability lobe model and verification tests

Apply the SL model that was presented in the theoretical section and use the obtained parameters of MFCs, DS parameters, etc to predict the SBL diagram for milling process of the SKD11 hard steel. The predicted results of SBL diagrams are illustrated in Fig. 10.

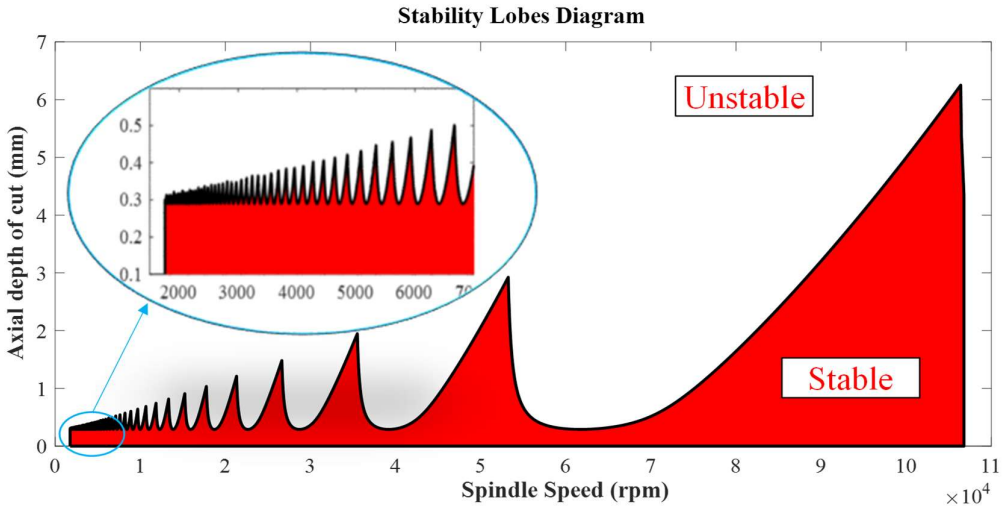

Fig.10. SBL diagram in Milling Process of SKD11 hard steel

Based on the SBL diagram in Fig. 10, it can be concluded that in this case, when milling the SKD11 hard steel using flat-end mill cutter, the width of the stability region increased when the spindle speed increased. The machining processes were almost at the stable conditions with the axial depth of cut to be smaller than 0.3 mm at all values of spindle speed.

The SBL model was verified by performing the milling tests. The milling tests were conducted at three values of spindle speed (2000 rpm, 4000 rpm, and 6000 rpm) with the constant of feed rate (200 mm/min), constant radial depth of cut (6 mm or slot cutting type). At each spindle speed, the values of axial cutting depth were selected from stable zone to unstable zone in SBL diagram (Fig. 10). The MFs and MVs were measured and analyzed to determine the stable and unstable milling conditions. Using the fast furrier transform (FFT), the MFs and MVs in time domain were transformed to the frequency domain (Fig. 11 and Fig. 12).

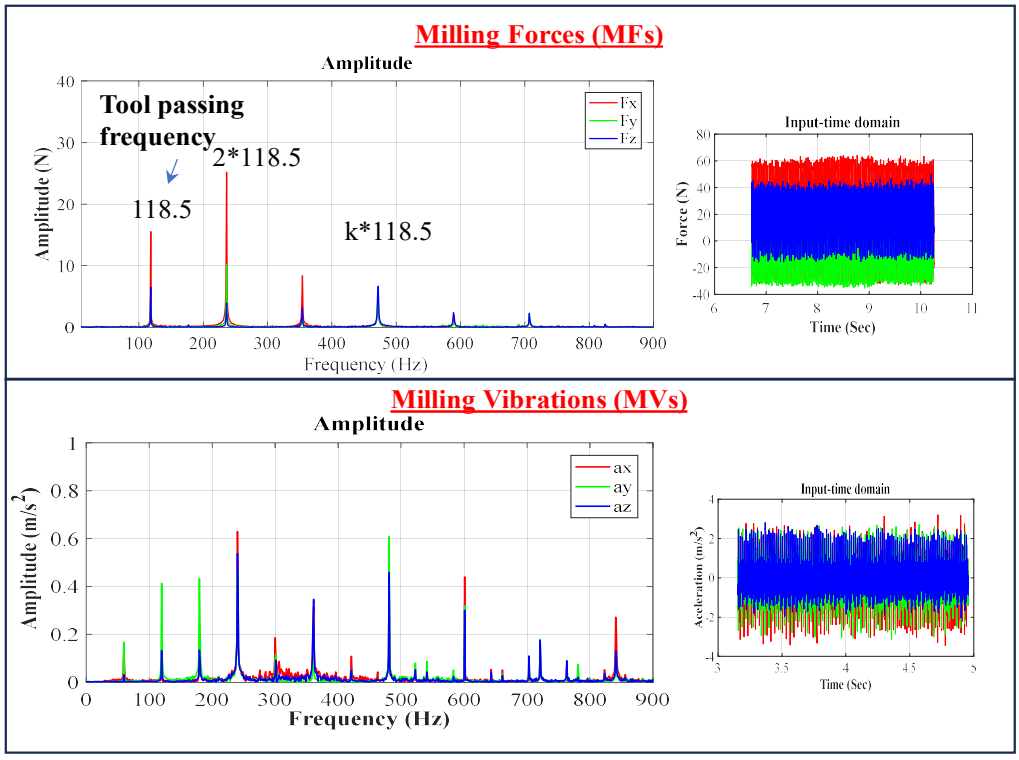

Fig.11. MFs and MVs at the stable condition

At the stable milling condition as shown in Fig. 11, the milling force frequency was almost an integer times the tool passing frequency $\omega_F = n^* \omega_T$ (where n is an integer). In these cases, the MFs and MCVs were also quite stable. However, at the unstable milling conditions, the MFs have different frequencies. The milling force has many different frequencies.

In which, the frequency values that equalled to the integer times of the tool pass frequency usually had a small amplitude, but the frequency value that was different from the integer times of the tool pass frequency had a very large amplitude (Fig. 12). In these cases, MFs and MVs had large volatility and were not stable.

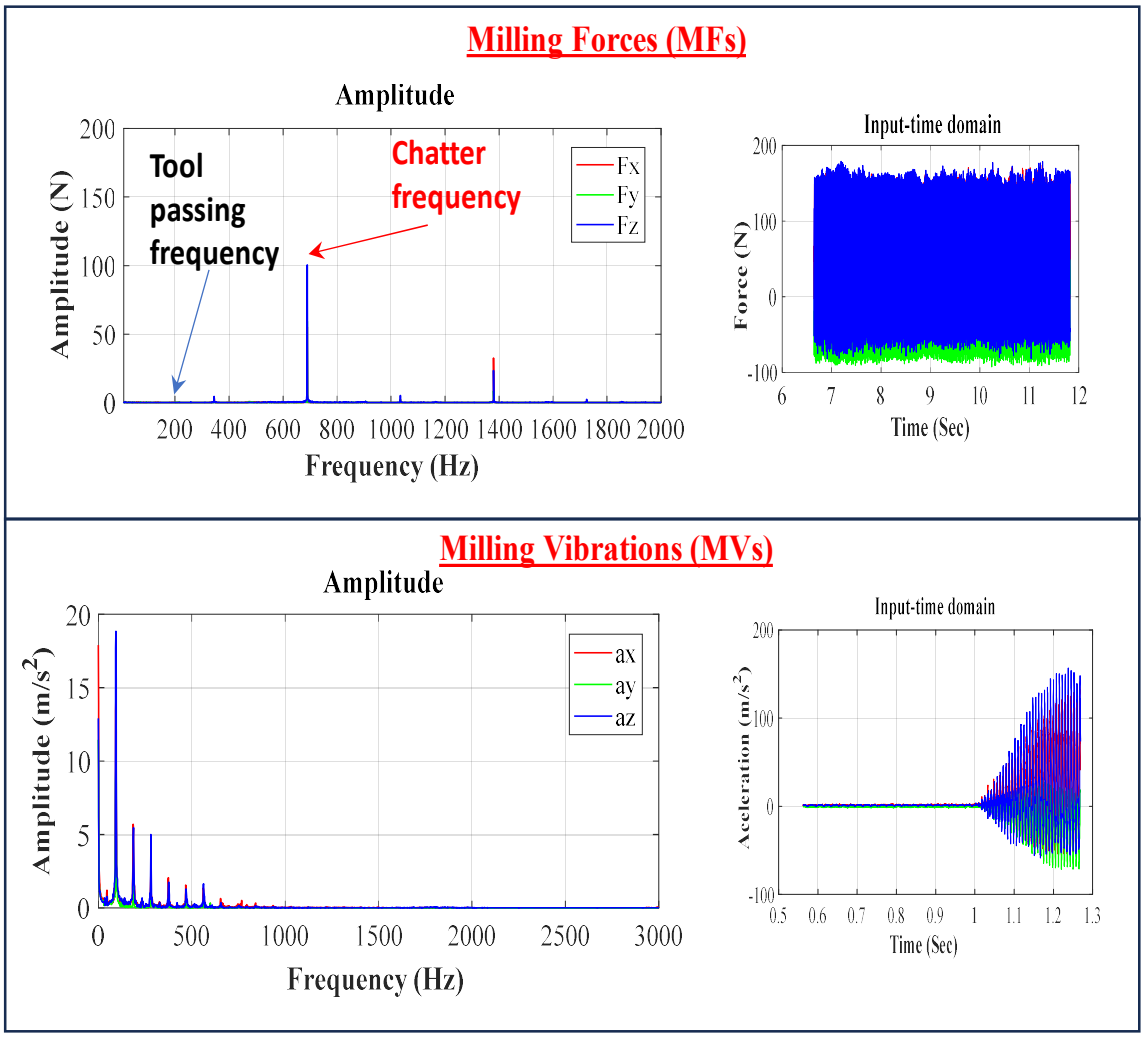

Fig.12. MFs and MVs at the unstable condition

Using this anlysis method, the stable and unstable conditions in milling processes were verified for all milling tests. The verified results were obtained and descried in Fig. 13. The verified results of the milling test in Fig. 13 show that the points that were selected in the stable zone had the verified results as the stable points.

The points that were selected at the unstable zone had the verified results as the unstable points. These obtained results represents the accuracy of the proposed model to predict the milling stable conditions.

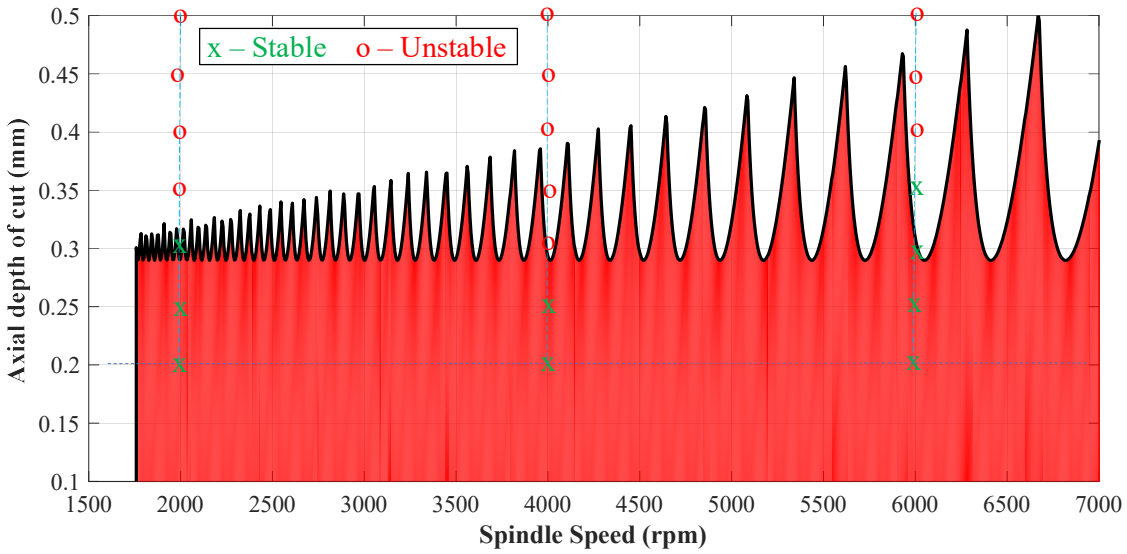

Fig.13. Verification of SBL model

However, the points that were selected at the border between stable and unstable zones, the verified results had some differences between the predicted results using the proposed model and the analyzed results from experimental processes (Fig. 13). These diferences can be explained that there are many other parameters that have not been included in the predictive model such as heat, tool wear, friction, etc. In addition, the accuracy in measuring structural parameters of machine-tool systems and machine-workpiece system cannot be assessed during the experimental process. Therefore, in the applying of the stable prediction results, it is the best way to choose the machining parameters at the absolute stable machining conditions.

5. Conclusion

This study was performed to investigated the mechanism and stability prediction of flat-end milling process of SKD11 hard steel. Several mechanism models were developed and proposed including static MF model, dynamic ML model, stability model. The values of MLCs and DSPs were determined based on the combination of theoretical and experimental method. The conlcusions that are drawn from this study are listed as following:

- the relationship was very close to the linear regression with high determination coefficients ($R^2 > 97\%$) in all three x, y, z directions.
- with each dynamic system, the natural frequencies of different directions were quite close to each other but different. The natural frequency of machine-tool system was almost half of natural frequency of machine-workpiece system.
- when milling the SKD11 hard steel using flat-end mill cutter, the width of the stability region increased when the spindle speed increased. The machining processes were almost at the stable conditions with the axial depth of cut to be smaller than 0.3 mm at all values of spindle speed.
- the stable and unstable conditions in milling processes were verified for all milling tests. The points that were selected in the stable zone had the verified results as the stable points. The points that were selected at the unstable zone had the verified results as the unstable points. The points that were selected at the border between stable and unstable zones, the verified

results had some differences between the predicted results using the proposed model and the analyzed results from experimental processes.

- these diferences can be explained that there are many other parameters that have not been included in the predictive model such as heat, tool wear, friction, etc. In addition, the accuracy in measuring structural parameters of machine-tool systems and machine-workpiece system cannot be assessed during the experimental process.
- in the applying of the stable prediction results, it is the best way to choose the machining parameters at the absolute stable machining conditions.

Acknowledgements

The authors thanks the support from Hanoi University of Industry, Vietnam with the university project No. 09-2022-RD/HĐ-ĐHCN.

References

[1]. Altintas, Y. Manufacturing automation: metal cutting mechanics, machine tool vibrations, and CNC design. Cambridge university press, 2012.

[2]. Tony L. Schmitz, K. Scott Smith. Machining Dynamics: Frequency Response to Improved Productivity, second edition, Springer Cham, 2019.

[3]. Cheng, K. Machining dynamics: fundamentals, applications and practices. Springer Science & Business Media, 2008.

[4]. Navarro-Devia, J. H., Chen, Y., Dao, D. V., & Li, H. Chatter detection in milling processes—a review on signal processing and condition classification. The International Journal of Advanced Manufacturing Technology, 2023, 125(9-10), 3943-3980.

[5]. Hashimoto, M., Marui, E., & Kato, S. Experimental research on cutting force variation during regenerative chatter vibration in a plain milling operation. International Journal of Machine Tools and Manufacture, 1996, 36(10), 1073-1092.

[6]. Toh, C. K. Vibration analysis in high speed rough and finish milling hardened steel. Journal of Sound and Vibration, 2004, 278(1), 101-115.

[7]. Y. Altintas, M. Weck. Chatter stability of metal cutting and grinding, CIRP Ann, 2004, 53, 619–642.

[8]. Y. Altintas, E. Budak, Analytical prediction of stability lobes in milling, CIRP Ann, 1995, 44, 357–362.

[9]. Y. Altintas, M. Eynian, H. Onozuka, Identification of dynamic cutting force coefficients and chatter stability with process damping, CIRP Ann, 2008, 57, 371–374.

[10]. Munoa J, Beudaert X, Dombovari Z, Altintas Y, Budak E, Brecher C. Chatter suppression techniques in metal cutting. CIRP Ann-Manuf Techn, 2016, 65(2):785–808.

[11]. Quintana G, Ciurana J. Chatter in machining processes: a review. Int J Mach Tool Manuf, 2011, 51(5), 363–76.

[12]. Grossi N, Sallese L, Scippa A, Campatelli G. Chatter stability prediction in milling using speed-varying cutting force coefficients. Procedia CIRP, 2014, 14, 170–5.

[13]. Ding Y, Zhu LM. Investigation on chatter stability of thin-walled parts considering its flexibility based on finite element analysis. Int J Adv Manuf Technol, 2016, 1–15.

[14]. Song QH, Liu Z, Wan Y, Ju GG, Shi JH. Application of Sherman-Morrison-Woodbury formulas in instantaneous dynamic of peripheral milling for thin-walled component. Int J Mech Sci, 2015, 96, 79–90.
[15]. Shi JH, Song QH, Liu ZQ, Ai X. A novel stability prediction approach for thin-walled component milling considering material removing process. Chin J Aeronaut, 2017, 30(5), 1789–98.
[16]. Zheng, J., Zhang, Y., & Qiao, H. Milling Mechanism and Chattering Stability of Nickel-Based Superalloy Inconel 718. Materials, 2023, 16(17), 5748.
[17]. Rusinek, R., & Lajmert, P. Chatter detection in milling of carbon fiber-reinforced composites by improved Hilbert–Huang transform and recurrence quantification analysis. Materials, 2020, 13(18), 4105.
[18]. Moradi, H., Movahhedy, M. R., & Vossoughi, G. Dynamics of regenerative chatter and internal resonance in milling process with structural and cutting force nonlinearities. Journal of Sound and Vibration, 2012, 331(16), 3844-3865.
[19]. Kao, Y. C., Nguyen, N. T., Chen, M. S., & Su, S. T. A prediction method of cutting force coefficients with helix angle of flat-end cutter and its application in a virtual three-axis milling simulation system. The International Journal of Advanced Manufacturing Technology, 2015, 77, 1793-1809.
[20]. Tung, N. N. Modeling of the Machining Dynamics: Cutting forces and Machining Characteristics in Three-Axis Milling Processes. Science and Technics Publishing House, 2020.